Coupled resonant modes in twisted acoustic metamaterials

Ying Cheng, Xiaojun Liu*

Key Laboratory of Modern Acoustics, Nanjing University, Nanjing 210093, China
*corresponding author, E-mail: liuxiaojun@nju.edu.cn

Abstract

Acoustic metamaterials constructed by resonant microelements in subwavelength scale were generally characterized by the effective medium approximation theory, which neglects the interaction between adjacent elements. In this paper, we show that twisting the orientation of resonators in acoustic metamaterials produces secondary coupled resonant modes by introducing internal vibration interaction. Metamaterials composed of single-slit Helmholtz resonator arranged in two-dimensional square lattice are investigated. We rotate a portion of the resonator so that the adjacent resonators in ΓX direction have a twist angle of φ. For the system with φ = 180°, the coupling interaction produces the symmetric coupled mode in in-phase oscillation and the anti-symmetric coupled mode in out-of-phase oscillation. This acoustic analog of "hybridization effect" leads to a sharp transparency window in the extended locally-resonant forbidden gap, which is analogous to the phenomenon of electromagnetically induced transparency. Such coupled resonant modes may have potential applications in sound wave manipulations such as acoustic filtering and imaging.

1. Introduction

Recently, acoustic metamaterials have received high interest due to their unprecedented physical behavior beyond those found in nature [1, 2]. In particular, the effective bulk modulus and mass density can be simultaneously or independently negative within a certain frequency region, which is unattainable using traditional composites. These intriguing properties allows ability to control sound in novel ways, ranging from acoustic cloaking [3-5] and subwavelength imaging [6-10] to sound energy superabsorption [11]. Most of the acoustic metamaterials reported to date are based on localized resonance induced by the subwavelength microelements. Negative effective bulk modulus and mass density can derive from appropriate monopolar and dipolar resonance, respectively [12]. One famous example is the engineered acoustic metamaterial consisting of Helmholtz resonator (HR), which is a tiny structure featuring a miniature gap analogous to the metal split-ring resonator in electromagnetic metamaterials [13]. Unique properties such as low-frequency locally-resonant band gap and anomalous transmission behavior have been demonstrated theoretically and experimentally [10, 14-17], and further numerical retrieval analysis of transmission-reflection coefficients also confirms the negative bulk modulus in one-dimensional HR chain and two-dimensional HR array [18-20]. Subsequent researches observe negative refraction, surface modes and superlensing effect via homogenization near resonance in a finite array of HRs [9, 10, 15].

The acoustic metamaterials derive their overall properties from individual sub-wavelength resonators. Changing the size and geometry of the HR determines the acoustic properties of the metamaterial and its operation frequency. The general case of describing an acoustic metamaterial uses the effective media approximation (EMA) theory [1, 14]. In EMA model, since the resonator element is much smaller in size than the working wavelength, the response of the acoustic metamaterial is treated as the averaged effects of the individual element's resonance response. Thus the metamaterial can be characterized by the effective parameters of mass density and bulk modulus.

However, the EMA theory ignores the coupling interactions between the resonator elements, which always exist when the elements are structured into metamaterials. Previous studies demonstrate that parallel HRs with identical resonant frequency could couple with each other, and the intensive interaction between adjacent HRs significantly extends the width of the locally-resonant forbidden gap, which is different from the case in solid elastic metamaterials [21]. The aim of our work is to demonstrate the coupled resonant modes in twisted acoustic metamaterials. In this paper, significant modulation to the band structure is investigated using the analyses of the dispersion curves and the transmission spectra. We identify these coupled resonances through the pressure fields of the supercell's eigenmodes. The adjunct resonator elements oscillate in-phase for the symmetric coupled mode and out-of-phase for the anti-symmetric coupled mode. These coupled resonant modes further lead to some "hybridization effect", which split the dispersion curves and causes the occurrence of sharp transparency window in the extended forbidden gap. This kind of coupled resonant mode may be used to develop novel functional acoustic devices in the future, including acoustic imaging with deep subwavelength resolution and acoustic transparency.

2. Description of the model

Figures 1(a) and 1(b) illustrates the schematic configuration of the regular acoustic metamaterial and the proposed twisted metamaterial. The cut-off view of the samples in *x*-*y* plane and the schematics of the corresponding supercells are plotted in the upper and lower panels, respectively. The structure we investigated is comprised of identical HRs periodically arranged in square lattice. The HRs are cylindrical metal shells with single slit. The outer and inner radii of the shells are a and b, respectively. The lattice constant is d and the height of the slit is h. The system is translationally invariant in the z-direction. The host medium is fluid such as water with bulk modulus κ_0 and mass density ρ_0, and the HRs are assumed as rigid-walled due to the mismatched acoustic impedance between metal and fluid. A supercell contains two HRs aligned along the x axis and the right HR is rotated with twist angle of φ [φ = 0° for regular metamaterial in Fig. 1(a) and φ = 180° for twisted metamaterial in Fig.1 (b)].

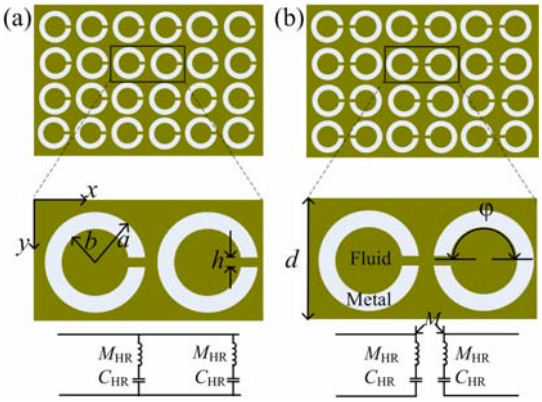

Figure 1: Scheme diagram and the corresponding equivalent acoustic circuit of (a) the regular acoustic metamaterials with φ = 0° and (b) the twisted acoustic metamaterials with φ = 180°.

Let us now consider the behavior of the individual HR. Since the incident wavelength is considerably long compared with the HR's transverse dimensions in *x*-*y* plane, we can employ the well-known theory of equivalent acoustic circuits to model the acoustic metamaterials. For simplicity, we use the 2D model. Figure 1(a) shows a circuit section composed of standard *L*-*C* oscillating circles, and the repeated circuit sections will further construct an acoustic transmission line in *x*-direction. The short slit of the split ring acts as an inductor with acoustic mass $M_{HR}=\rho_0*(a-b)/h$, and the inner cavity acts as a capacity with acoustic capacitance $C_{HR}=\pi b^2/\rho_0 c_0^2$. In all our studies, the host medium is chosen as water with κ_0 = 2.19 GPa and ρ_0 = 998 kg/m^3, and the geometry size of the resonator is set as a=0.48 m, b=0.34 m, h=0.05 m and d=1 m unless otherwise specified. To include the influence of periodicity on the acoustic radiation of the slit, we employ an equivalent extra mass radiation mass and revise the effective acoustic mass as $M_{eff}=\rho_0(a-b+2.85h)/h$. Hence the resonant frequency f_R [$=(1/M_{eff}C_{HR})^{0.5}/(2\pi)$] of the HR is obtained to be 164 Hz, and the corresponding normalized frequency $f_R d/c_0$ is 0.11. The HR chain in *x*-direction could be modeled as a 1D transmission line with periodic loaded *L*-*C* shunt branches. We further give a qualitative description on the coupling effect from the view point of acoustic circuit. Due to the twisted configuration, the near-field coupling interaction between close-spaced slits is significant enhanced and its influence could be characterized as an mutual acoustic mass M. M takes negative value when the two HRs oscillate in-phase since the mass loading at the outlet of the slit is decreased, and vice versa. Thus a coupled acoustic propagation mode may be established in this case and could be used to open a transparency window in forbidden gap, as illustrated below.

3. Results and discussion

3.1. Band structures

To describe the coupling properties for acoustic wave propagating within the twisted structure, we first calculate the band structure of the metamaterials. The band structure of the composite metamaterial can be calculated by solving the acoustic eigenvalue problem of the supercell. The periodic boundary conditions are applied to the supercell along the *x*-direction and *y*-direction based on Bloch's theorem. The finite element technique transforms the wave equation into a generalized acoustic eigenvalue problem expressed by $[K(k_x)-\omega^2 M]P=0$, where $K(k_x)$ and M are the stiffness and mass matrices. An alternative searching arithmetic is employed to determine the eigenfrequency ω. The spatial discretization is fine enough for the convergence in our numerical experiments.

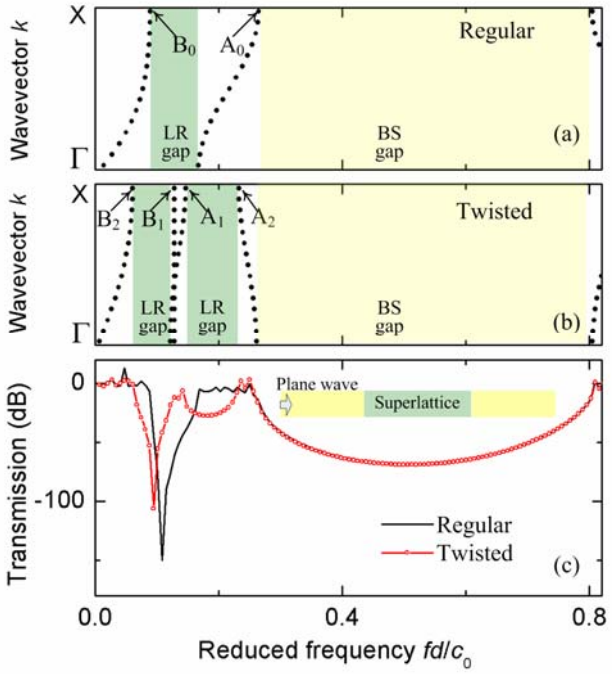

Figure 2: Band structures for (a) regular and (b) twisted acoustic metamaterials. The corresponding normalized transmission spectra are shown in panel (c).

The band structures for regular and twisted metamaterials are shown in Figs. 2(a) and 2(b), respectively. As a first observation, we can see one Bragg-scattering (BR) gap from 0.256 to 0.808 and one locally-resonant (LR) gap from 0.089 ~ 0.167 for regular acoustic metamaterials with $\varphi = 0°$. The phenomenon is consistent with previous studies for regular HR chain and array [14, 15, 21]. In contrast, although the position and width of the BR gap for twisted metamaterial are exactly the same as that for regular metamaterial, the number of transmission bands below BR gap is doubled. Generally, two native bands separated by the only LR gap exist in the frequency range below the BR gap for regular metamaterial [Fig. 2(a)], which originate from the eigen-vibration of the individual HRs. However, four transmission bands intersected by two LR gaps exist in the frequency region below the BR gap for the twisted case [Fig. 2(b)]. The origin of the four transmission bands could be ascribed to the symmetric and asymmetric combination of original eigen-vibration modes by the intensive coupling interaction, which will be discussed in the following section. The calculations assume that the dissipation is weak and the vibration amplitude is limited, hence the viscosity loss is not included in this case. We also take the large loss factor into consideration and find that the band structures change a little.

In order to confirm the analysis of band structures, the transmission spectra through finite supercells are calculated using the full-wave finite element simulations. The computational domain is shown in the inset of Fig. 2(c). Bloch conditions are applied in the y-direction since the structure is supposed to be infinite in this direction. A plane wave source with the amplitude of 1 Pa is added on the left surface of the domain. In order to improve the accuracy of the numerical model, the perfect match layers are added at the external boundaries to simulate the infinite region. Sound wave transmissions through the periodic superlattice are calculated, as shown in Fig. 2(c). We note that the LR transmission gap appears at 0.089 ~ 0.167 for the case of regular acoustic metamaterials, which is in agreement with the dispersion curves [as shown in Fig. 2(a)]. On the other hand, the LR gaps appear at 0.060 ~ 0.121 and 0.146 ~ 0.233 for the case of twisted acoustic metamaterials. Note that a narrow transparency window extends from 0.121 to 0.146 which located between the two LR gaps [see Fig. 2(b)]. This secondary transparency window should be attributed to the splitting of the dispersion curves. We also note that both BR gaps appear at 0.256 ~ 0.808 for the two cases. In general, the transmission spectra are in agreement with the dispersion curves. The consistency demonstrates the drastic effect of subwavelength coupling interaction on the propagation of acoustic waves.

We continue to study the transparency window inside the extended LR gap through the pressure field of wave propagation. The edge of third dispersion curve is utilized as load frequency since only one eigenmode is supported in this case. The pressure fields at the load frequencies of 200 Hz for the two cases are shown in Figs. 3(a) and 3(b), respectively. For comparison, the corresponding profile along the cross-section line of $y=d/2$ are plotted in each panel. Since the frequency of incident wave is inside the LR gap for the case of regular metamaterials, the incident wave could only penetrate the first few HRs and the interior field is nearly zero. In this case, the propagation of the wave is forbidden, and most of the incident energy is reflected backward. These results are consistent with the dispersion curves and transmission spectra. On contrary, the incident wave could effectively propagate through the superlattice for the case of twisted metamaterials. The variation trend of the absolute value of the pressure field is periodic, which can be determined by the periodicity of the supercell. In this case, the supercells exhibit unique oscillation modes in which the two HRs in each supercell vibrate in-phase with each other. Note that the pressure amplitude in the supercell region is significantly higher than that of the incident and transmitted wave. This phenomenon should be attributed to the intensive resonance in the HRs through coupling interaction. This finding should have substantial practical applications, for example in controlling and filtering the propagation wave via tuning the twisted structure.

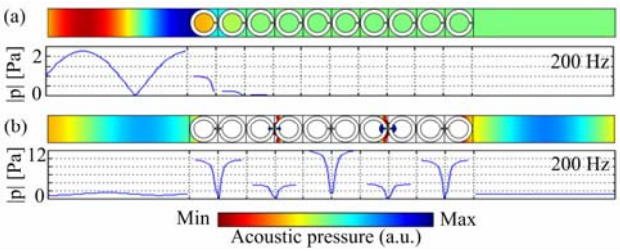

Figure 3: Pressure fields and the corresponding profile along the cross-section line of $y=d/2$ at the load frequency of 200 Hz for (a) regular and (b) twisted acoustic metamaterials. The red (blue) corresponds to the maximum (minimum) pressure. The plane wave with the amplitude of 1 Pa travels along the x-direction.

It is interesting to note that the acoustic transparency window induced by coupled resonance is different from that induced by coupling between the rod-resonator modes [22], although both structures employ twisted configuration. In the rod-resonators with a twist angle of 45° relative to each other, the surface resonant modes with identical resonant frequencies but different quality factors respectively act as radiative mode and dark mode, and the destructive interference of them results in electromagnetically-induced-transparency like effect. Importantly, the distance of the rod-resonators is much longer than the wavelength. In contrast, the HRs in our proposal can be deep subwavelength spaced, which is very compact for construction. The transparency is achieved through the cancellation of opposite contributions from the two HRs.

3.2. Eigenmodes distributions

In order to explore the physical mechanism causing such splitting of the dispersion curves illustrated in Fig. 2, we further investigate the recombination of acoustic vibration modes induced by the twisted structure. Sound waves in the metamaterials propagate through the particle vibrations in the constructive resonant microelements in subwavelength

scale, which can be decomposed into eigenmodes with the characteristic oscillation pattern. In this section, we characterize the eigenmodes through the pressure field distribution of the supercell. By assigning both the wave-vector k_x and frequency ω, the specific eigenmodes are excited and the pressure data at each node are recorded to reconstruct the eigenmodes. The eigenmodes defined at the zone edge below the BS gap are discussed. We have also investigated the other modes with k values located at general positions of the dispersion curves, e.g. at zone center. The results show that the coupling interaction maintains the effect of mode recombination, which are not listed in the paper.

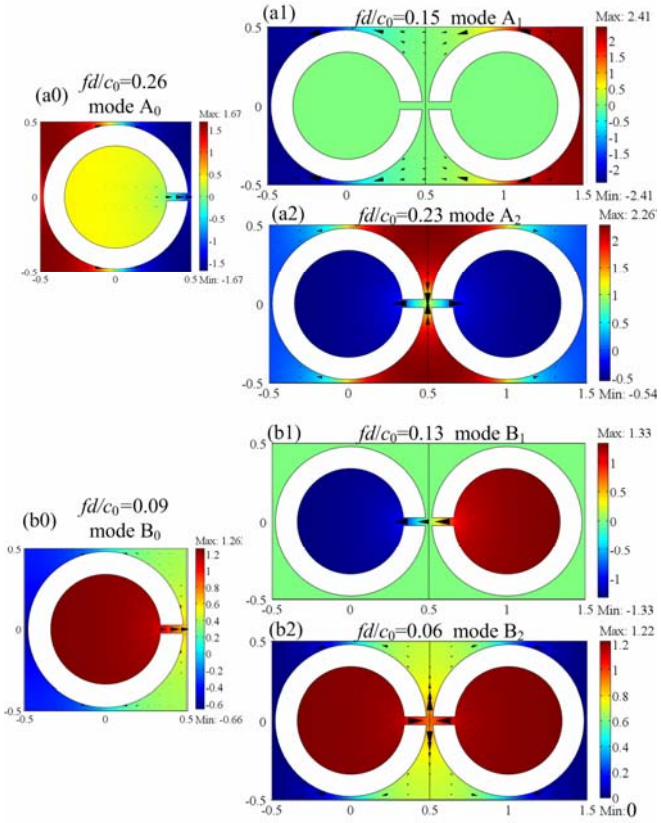

Figure 4: Pressure field distributions of the eigenmodes. Panels (a0) and (b0) correspond to modes A_0 and B_0 for the regular acoustic metamaterials, and panels (a1), (a2), (b1) and (b2) correspond to modes A_1, A_2, B_1 and B_2 for the twisted acoustic metamaterials. The direction (size) of the cones indicates the direction (magnitude) of velocity vector, and the red (blue) correspond to the maximum (minimum) pressure.

Based on the mode characterization method, we first depict the pressure fields of the eigenmodes A_0 [marked in Fig. 2(a)] for regular acoustic metamaterials with the twist angle of $\varphi = 0°$ in Fig. 4(a0). In this case, the dominant particle motion occurs in the short neck, and the upper/lower region outside the resonator. The pressure distribution exhibits symmetric variation with respect to the mid-plane of the short-neck (the plane of $y = d/2$). Note that the eigenmodes are defined at the zone edge with $k_x d/\pi = 1$ and $\lambda = 2d$, for which the adjacent unit cells move in antiphase.

Comparing mode A_0 with mode A_1 and A_2 for the twisted acoustic metamaterials with $\varphi = 180°$ [see Figs. 4(a1) and 4(a2)], an interesting observation is that the oscillation of the adjacent cells exhibit in both in-phase and out-of-phase patterns. For the case of mode A_1, the left and right HRs exhibit in-phase vibration along the x-direction [Fig. 4(a1)]. As a result, the entire supercell also shows antisymmetric pressure field distribution with respect to the mid-plane along x-direction (the plane of $x = d$). In contrary, the left and right HRs vibrate out of phase for the case of mode A_2, leading to the symmetric variation of the pressure field [Fig. 4(a2)]. Therefore, the twisted structure combines the vibration mode of standalone HR into a pair of asymmetric and symmetric modes, which is analogous to the bonding and anti-bonding magnetic plasmon modes in magnetic dimer [23]. Similar effect of eigenmode recombination is also found in other transmission band. For example, the mode B_0 [Fig. 3(b0)] constructs the symmetric mode B_1 [Fig. 4(b1)] and antisymmetric mode B_2 [Fig. 5(b2)]. We outline the physical mechanism which leads to the combination effect as follows. The hybridization of the acoustic response in the case of $\varphi = 180°$ is mainly due to vibration coupling between the HRs. Each HR in deep subwavelength scale can be viewed as a quasi-atom, and the supercell of the coupled metamaterial with $\varphi = 180°$ can be regarded as a quasi-molecule. The quasi-atom possesses strong polarity caused by its nonaxisymmetrical structure, and the local amplitude at the short neck may be extremely high. For regular metamaterial with $\varphi = 0°$, the polar axes of all of the HRs lie in the same direction, and the interactions between adjacent cells are so weak that the periodic cells vibrate in-phase independently [as shown in Fig. 3(a)]. On contrary, for twisted metamaterial with $\varphi = 180°$, the polar axes of the two HRs in the quasi-molecule lie in opposite direction, and the significantly enhanced interaction couples the left and right HRs without obvious modification to their standalone eigenmodes. The decoupled eigenmode A_0 can combine in symmetric and asymmetric manners, leading to the splitting of the dispersion relations (e.g. the two transmission bands for regular acoustic metamaterials with $\varphi = 0°$ below the BR gap split into four transmission bands for twisted metamaterials with $\varphi = 180°$ as illustrated in Fig. 2). In general, the splitting of the dispersion curves originates from the hybridization of the original decoupled modes with small frequency offset.

3.3. Evolution of coupling effect with the lattice constant

As illustrated above, the coupling interaction is crucial in the hybridization effect of the transmission bands. The strength of the coupling interaction depends strongly on the distance between the quasi-atoms and for the considered geometry can be tuned by changing the lattice constant d. Therefore, we investigate the band structure with the lattice constant ranging from $d = 0$ to 1.6 m. The evolution of bandgap extent is extracted from the band structures and illustrated as a function of the lattice constant d in Fig. 5, where panels (a) and (b) correspond to the regular acoustic metamaterials with $\varphi = 0°$ and twisted acoustic metamaterials with $\varphi = 180°$, respectively. It is found that the sensitivity of the

bandgaps to the lattice constant is different. Three remarks should be noted. (1) Both BS gaps for the two cases (bounded by curves with blue open squares and blue open circles) gradually shrink in the same trend and the midgap frequencies move downward. Its upper (lower) band-edge frequency decreases from 0.80 (0.26) to 0.37 (0.23) when the lattice constant d is increased from 1 m to 1.6 m. This phenomenon, which is analogous to the BS gap in phononic-crystals composed of solid cylinders periodically arranged in the background of fluid, should be attributed to the fact that the periodicity of the scatterer has to be of the same length-scale as half the wavelength of the sound waves. (2) The width of the LR gap for the case of regular metamaterial also gradually shrinks. However, its midgap frequency eventually approaches 0.12, which is almost unchanged and equals the resonant frequency of the individual HR. (3) For the case of twisted metamaterial, similar dependence on the lattice constant is also observed in both the first and the second LR gap. In addition, the transparency window between the two LR gaps also depends on the lattice constant. Its upper edge frequency (indicated by curve with red solid up-triangles and) first slightly increases from 0.15 at d = 1 m to 0.16 at d = 1.1 m and then decreases to 0.13 at d = 1.6 m. Meanwhile, its lower edge frequency (indicated by curve with black solid circles) maintains the value of 0.12 which is almost unchanged.

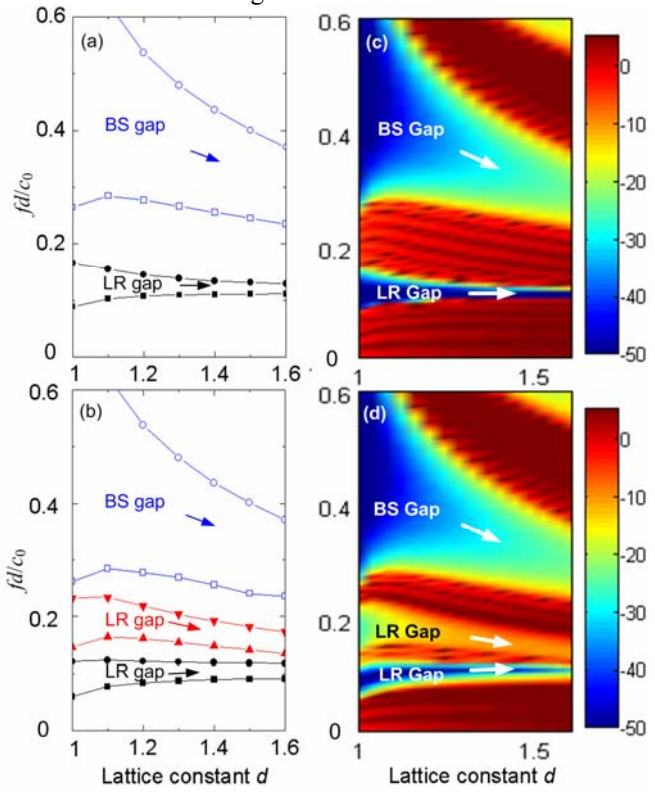

Figure 5: Complete phononic band gap extent as a function of the lattice constant for (a) regular and (b) the twisted acoustic metamaterials. The corresponding normalized transmission spectra are plotted in panels (c) and (d), respectively.

To confirm the bandgap extent in Figs. 5(a) and 5(b), the transmission spectra maps with the variation of the lattice constant are shown in Figs. 5(c) and (d). It is found that the location and width of transmission gaps agree with the band structures. In addition, the transparency window lies within the frequency region defined by the transmission bands of the infinite system. From above observations, we can conclude that the strength of the coupling interaction depends strongly on the lattice constant, which performs as a key factor in engineering the band gap and acoustic transparency window.

4. Conclusions

In conclusion, we have studied the coupled resonant modes in acoustic metamaterials composed of single-slit Helmholtz resonators with twist angle between adjacent cells. The coupling effects are demonstrated by the consistent band structures and transmission spectra, in which doubled dispersion curves and a sharp transparency window in the extended LR gap are observed. Due to the resonance interaction, eigen-vibration mode of individual HR recombined into a pair of symmetric coupled mode in in-phase oscillation and anti-symmetric coupled mode in out-of-phase oscillation. By adjusting the coupling strength which strongly depends on the separation distance determined by the lattice constant, transmission and modes of an acoustic metamaterial are highly tunable. Thus, the coupled resonant modes, introduced by twisting the orientation of resonators in acoustic metamaterial, may provide a new way of tailoring their acoustic properties.

Acknowledgements

This work was supported by the National Basic Research Program of China under Grant No. 2012CB921504, NSFC (11074124, 11104139 and 10904052), SRFDP 20110091120040, and Jiangsu Provincial Natural Science Foundation (BK2011542) and PAPD of Jiangsu higher education institutions.

References

[1] L. Fok, M. Ambati, X. Zhang, Acoustic metamaterials. *MRS Bull*. 33: 931-934, 2008.

[2] B. I. Popa, S. A. Cummer, Design and characterization of broadband acoustic composite metamaterials. *Phys. Rev. B* 80: 174303, 2009.

[3] S. Zhang, C. Xia, N. Fang, Broadband acoustic cloak for ultrasound waves. *Phys. Rev. Lett.* 106: 024301, 2011.

[4] N. Stenger, M. Wilhelm, M. Wegener, Experiments on Elastic Cloaking in Thin Plates. *Phys. Rev. Lett.* 108: 014301, 2012.

[5] Y. Cheng, F. Yang, J. Y. Xu, X. J. Liu, A multilayer structured acoustic cloak with homogeneous isotropic materials. *Appl. Phys. Lett.* 92: 151913, 2008.

[6] J. S. Li, L. Fok, X. B. Yin, G. Bartal, X. Zhang, Experimental demonstration of an acoustic magnifying hyperlens. *Nat. Mater.* 8: 931-934, 2009.

[7] C. M. Park, J. J. Park, S. H. Lee, Y. M. Seo, C. K. Kim, S. H. Lee, Amplification of Acoustic Evanescent Waves Using Metamaterial Slabs. *Phys. Rev. Lett.* 107: 194301, 2011.

[8] X. Y. Ao, C. T. Chan, Far-field image magnification for acoustic waves using anisotropic acoustic metamaterials. *Phys. Rev. E* 77: 025601, 2008.

[9] M. Farhat, S. Guenneau, S. Enoch, A. B. Movchan, Negative refraction, surface modes, and superlensing effect via homogenization near resonances for a finite array of split-ring resonators. *Phys. Rev. E* 80: 046309, 2009.

[10] S. Zhang, L. L. Yin, N. Fang, Focusing ultrasound with an acoustic metamaterial network. *Phys. Rev. Lett.* 102: 194301, 2009.

[11] R. Q. Li, X. F. Zhu, B. Liang, Y. Li, X. Y. Zou, J. C. Cheng, A broadband acoustic omnidirectional absorber comprising positive-index materials. *Appl. Phys. Lett.* 99: 193507, 2011.

[12] J. Li, C. T. Chan, Double-negative acoustic metamaterial. *Phys. Rev. E* 70: 055602, 2004.

[13] D. R. Smith, Willie J. Padilla, D. C. Vier, S. C. Nemat-Nasser, S. Schultz, Composite medium with simultaneously negative permeability and permittivity. *Phys. Rev. Lett.* 84: 4184-4187, 2000.

[14] N. Fang, D. J. Xi, J. Y. Xu, M. Ambati, W. Srituravanich, C. Sun, X. Zhang, Ultrasonic metamaterials with negative modulus. *Nat. Mater.* 5: 452-456, 2006.

[15] S. Guenneau, A. Movchan, G. Petursson, S. A. Ramakrishna, Acoustic metamaterials for sound focusing and confinement. *New J. Phys.* 9: 399, 2007.

[16] A. B. Movchan, S. Guenneau, Split-ring resonators and localized modes. *Phys. Rev. B* 70: 125116, 2004.

[17] Z. G. Wang, S. H. Lee, C. K. Kim, C. M. Park, K. Nahm, S. A. Nikitov, Effective medium theory of the one-dimensional resonance phononic crystal. *J. Phys.-Condens. Mat.* 20: 055209, 2008.

[18] V. Fokin, M. Ambati, C. Sun, X. Zhang, Method for retrieving effective properties of locally resonant acoustic metamaterials. Phys. Rev. B 76: 144302, 2007.

[19] S. H. Lee, C. M. Park, Y. M. Seo, Z. G. Wang, C. K. Kim, Composite acoustic medium with simultaneously negative density and modulus. *Phys. Rev. Lett.* 104: 054301, 2010.

[20] Y. Cheng, J. Y. Xu, X. J. Liu, One-dimensional structured ultrasonic metamaterials with simultaneously negative dynamic density and modulus. *Phys. Rev. B* 77: 045134, 2008.

[21] Y. Cheng, J. Y. Xu, X. J. Liu, Broad forbidden bands in parallel-coupled locally resonant ultrasonic metamaterials. *Appl. Phys. Lett.* 92: 051913, 2008.

[22] F. Liu, M. Ke, A. Zhang, W. Wen, J. Shi, Z. Liu, P. Sheng, Acoustic analog of electromagnetically induced transparency in periodic arrays of square rods. *Phys. Rev. E* 82: 026601, 2010.

[23] H. Liu, D. A. Genov, D. M. Wu, Y. M. Liu, Z. W. Liu, C. Sun, S. N. Zhu, X. Zhang, Magnetic plasmon hybridization and optical activity at optical frequencies in metallic nanostructures. *Phys. Rev. B* 76: 064304, 2007.